Stimulus frequency modulates brainstem response to respiratory-gated transcutaneous auricular vagus nerve stimulation

Roberta Sclocco [a, b, *], Ronald G. Garcia [a, c, d], Norman W. Kettner [b], Harrison P. Fisher [a], Kylie Isenburg [a], Maya Makarovsky [a], Jessica A. Stowell [c], Jill Goldstein [a, c, e], Riccardo Barbieri [f, g], Vitaly Napadow [a, b]

[a] Athinoula A. Martinos Center for Biomedical Imaging, Department of Radiology, Massachusetts General Hospital, Harvard Medical School, Charlestown, MA, USA
[b] Department of Radiology, Logan University, Chesterfield, MO, USA
[c] Department of Psychiatry, Massachusetts General Hospital, Harvard Medical School, Boston, MA, USA
[d] School of Medicine, Universidad de Santander (UDES), Bucaramanga, Colombia
[e] Department of Obstetrics and Gynecology, Massachusetts General Hospital, Harvard Medical School, Boston, MA, USA
[f] Department of Electronics, Information and Bioengineering, Politecnico di Milano, Italy
[g] Department of Anesthesia, Critical Care and Pain Medicine, Massachusetts General Hospital, Harvard Medical School, Boston, MA, USA

ARTICLE INFO

ABSTRACT

Background: The therapeutic potential of transcutaneous auricular VNS (taVNS) is currently being explored for numerous clinical applications. However, optimized response for different clinical indications may depend on specific neuromodulation parameters, and systematic assessments of their influence are still needed to optimize this promising approach.
Hypothesis: We proposed that stimulation frequency would have a significant effect on nucleus tractus solitarii (NTS) functional MRI (fMRI) response to respiratory-gated taVNS (RAVANS).
Methods: Brainstem fMRI response to auricular RAVANS (cymba conchae) was assessed for four different stimulation frequencies (2, 10, 25, 100 Hz). Sham (no current) stimulation was used to control for respiration effects on fMRI signal.
Results: Our findings demonstrated that RAVANS delivered at 100 Hz evoked the strongest brainstem response, localized to a cluster in the left (ipsilateral) medulla and consistent with purported NTS. A co-localized, although weaker, response was found for 2 Hz RAVANS. Furthermore, RAVANS delivered at 100 Hz also evoked stronger fMRI responses for important monoamine neurotransmitter source nuclei (LC, noradrenergic; MR, DR, serotonergic) and pain/homeostatic regulation nuclei (i.e. PAG).
Conclusion: Our fMRI results support previous localization of taVNS afference to pontomedullary aspect of NTS in the human brainstem, and demonstrate the significant influence of the stimulation frequency on brainstem fMRI response.

Introduction

Transcutaneous auricular vagus nerve stimulation (taVNS) has enjoyed renewed interest in recent years since its description almost twenty years ago as a non-invasive approach to vagus nerve stimulation through the auricular branch of the vagus nerve (ABVN). Multiple clinical disorders have been targeted by taVNS researchers, including epilepsy [1], depression [2,3], pain [4–8], stroke [9,10], and various gastrointestinal [11,12] and cardiovascular disorders [13–18]. Importantly, stimulation parameter optimization may differ between these clinical applications, and an objective framework should be explored for optimizing parameter setting for taVNS.

Towards identifying potential biomarkers, recent basic research efforts have focused on gaining a more thorough understanding of the physiological mechanisms supporting clinical taVNS outcomes (as reviewed in Kaniusas et al. [19,20]). For instance, non-invasive human neuroimaging using functional magnetic resonance imaging (fMRI) has been applied to assess brainstem response to taVNS

* Corresponding author. 149 13th St, 02129, Charlestown, MA, USA.
E-mail address: roberta@nmr.mgh.harvard.edu (R. Sclocco).

in the nucleus tractus solitarii (NTS), a thin longitudinal nucleus located in the dorsal medulla, and the primary synapse for vagal afference [7,21–27]. While neuroimaging methods in these studies have varied, taVNS has been demonstrated to consistently activate purported ipsilateral NTS at the pontomedullary junction, and, via ascending projections, locus coeruleus (LC), periaqueductal gray (PAG), and pontine raphe nuclei in the brainstem, thalamus, and a widespread network of higher cortical regions including cingulate and prefrontal cortices (as reviewed in Badran et al. [24]). However, we should also note that prior taVNS fMRI studies employed wide variability in stimulation designs, from the choice of anatomical target [23] and control site [28,29], to stimulation parameters determining dose, such as burst duration time, pulse width, and frequency. Variability between studies also likely stems from important imaging parameters, such as spatial resolution, which is critical for imaging the very small volume nuclei of the brainstem [30,31].

Our own studies have described another, less commonly explored stimulation parameter, respiratory phase of stimulation, finding that stimulation during the exhalatory phase produced more robust NTS, as well as locus coeruleus and raphe nuclei response in the brainstem [7,26]. While Respiratory-gated Auricular Vagal Afferent Nerve Stimulation (RAVANS) has been found to enhance brainstem targeting for taVNS, parameter optimization within this framework with other important stimulus variables, such as burst frequency, are unknown.

Our current well-powered study explored sensitivity in fMRI brainstem response to this more commonly modulated parameter, stimulation frequency. We applied multiband fMRI for improved spatiotemporal resolution and specifically evaluated ipsilateral medullary, as well as LC, raphe, and PAG nuclei response to RAVANS taVNS.

Methods

We completed a cross-over neuroimaging study at the Athinoula A. Martinos Center for Biomedical Imaging, Department of Radiology, Massachusetts General Hospital (MGH), in Boston, MA. All study protocols were approved by MGH and Partners Human Research Committee and all subjects provided written informed consent.

Subjects

Thirty (30) healthy adult subjects (17 female, age: 29.0 ± 9.8 years, mean $\pm$ SD) were enrolled. Exclusion criteria included major neurological or other medical disorders that would interfere with study procedures or confound results (e.g. conditions altering blood flow), a history of seizure or significant head trauma, a history of Axis I psychiatric diagnosis, as well as any contraindication for MRI.

Experimental protocol

Participants were first familiarized with taVNS stimulation and instructed prior to fMRI imaging during an intensity calibration procedure using the method of limits. Specifically, they were asked to rate the intensity of stimulation on a numeric rating scale (NRS) ranging from 0 ("no sensation") to 10 ("pain threshold"). Stimulation intensity was aimed for a "moderately strong, but not painful sensation," corresponding to a target score of 4–5 on the 0–10 scale. As stimulation used the RAVANS taVNS procedure, participants were informed of the intermittent nature of stimulation, although no mention was made of respiration gating.

Each subject completed a single MRI session, consisting of five 8.5-min duration fMRI scan runs, including a no-stimulation control scan and four active stimulation scan runs. Specifically, an initial sham stimulation run (electrodes placed within the cymba conchae but no electrical current passed, performed first in order, to better maintain blinding) was followed by four active RAVANS scans, each using a different stimulation frequency (2 Hz, 10 Hz, 25 Hz, 100 Hz), with a randomized order across subjects. The four frequencies were chosen to span the range used in prior taVNS studies, including our own. Subject were asked to keep their eyes open and their head as still as possible during the scans.

Stimulation

RAVANS taVNS stimuli consisted of monophasic rectangular pulse burst trains with 300 μs pulse width and a train duration of 1.5 s, provided by a commercially available constant-current electrostimulation unit (UROstim, schwa-medico GmbH, Ehringshausen, Germany). Stimuli to the auricle were delivered using custom-built, ergonomically-shaped MR-compatible electrodes (Bionik Medical Devices, Bucaramanga, Colombia) placed within the cymba conchae of the left ear (Fig. 1A). Respiration was measured by a custom-built pneumatic belt placed around the subjects' lower thorax. Low compliance tubing connected the belt to a pressure transducer (PX138-0.3D5V, Omegadyne, Inc., Sunbury, OH, USA), and the voltage signal, reflecting respiratory volume, was recorded by a laptop-controlled device (National Instruments USB DAQCard 6009, 14-bit i/o, with LabView© 2017 data acquisition software). End-inhalation was detected in real-time based on an adaptive threshold detection algorithm, and a TTL signal was sent to a miniature high-frequency relay (G6Z-1P-DC5, Omron Electronics Components, Shaumburg, IL, USA), thereby controlling the onset and offset of each stimulation pulse train, which was set to begin after a 0.1 s delay from the end-inhalation timestamp, and last 1.5 s in duration. Stimulus intensity (current amplitude, mA) was percept-matched across subjects and across different stimulus frequency scan runs (targeting 4–5 on the 0–10 NRS reported above, Fig. 1B). Current amplitude was set just prior to each scan run, and intensity ratings (inquired as "average intensity" over the 8.5 min) were verbally assessed again at the end of each stimulation scan run, resulting in one rating per stimulation frequency (Fig. 1C). Potential differences in stimulation amplitudes and ratings across conditions were explored using repeated measure ANalyses Of VAriance (ANOVA) implemented in Matlab (R2016b, The MathWorks, Natick, MA, USA).

MRI and physiological data collection

Blood-oxygenation level-dependent (BOLD) fMRI data were collected on a Siemens 3T Skyra scanner (Siemens Healthineers, Erlangen, Germany) using a 64-channel head/neck coil. Whole-brain fMRI data were acquired with gradient-echo echo-planar imaging (EPI) using a Simultaneous Multi-Slice acquisition with multiband factor 5 and the following parameters: 2 mm isotropic voxel size (field of view = 200×200 mm^2), 75 axial slices, 2 mm slice thickness, repetition time (TR) = 1250 ms, echo time (TE) = 33 ms, flip angle = 65°, 8 dummy volumes automatically discarded, 400 time-series measurements. An additional volume was collected having opposite phase encoding, in order to estimate and correct susceptibility-induced distortion during pre-processing (topup, FSL). To aid co-registration, a high-resolution (1 mm isotropic voxel size) T1-weighted structural MRI scan was collected for each subject with a multi-echo MP-RAGE pulse sequence (TR = 2530 ms, TE1/TE2/TE3/TE4 = 1.69/3.55/5.41/7.27 ms, flip angle = 7°, field of view = 256×256 mm^2, 176 axial slices). Concurrent with BOLD data, cardiac pulse signal was recorded via blood pressure fluctuation using a piezo-electric pulse transducer, which provides a sharper
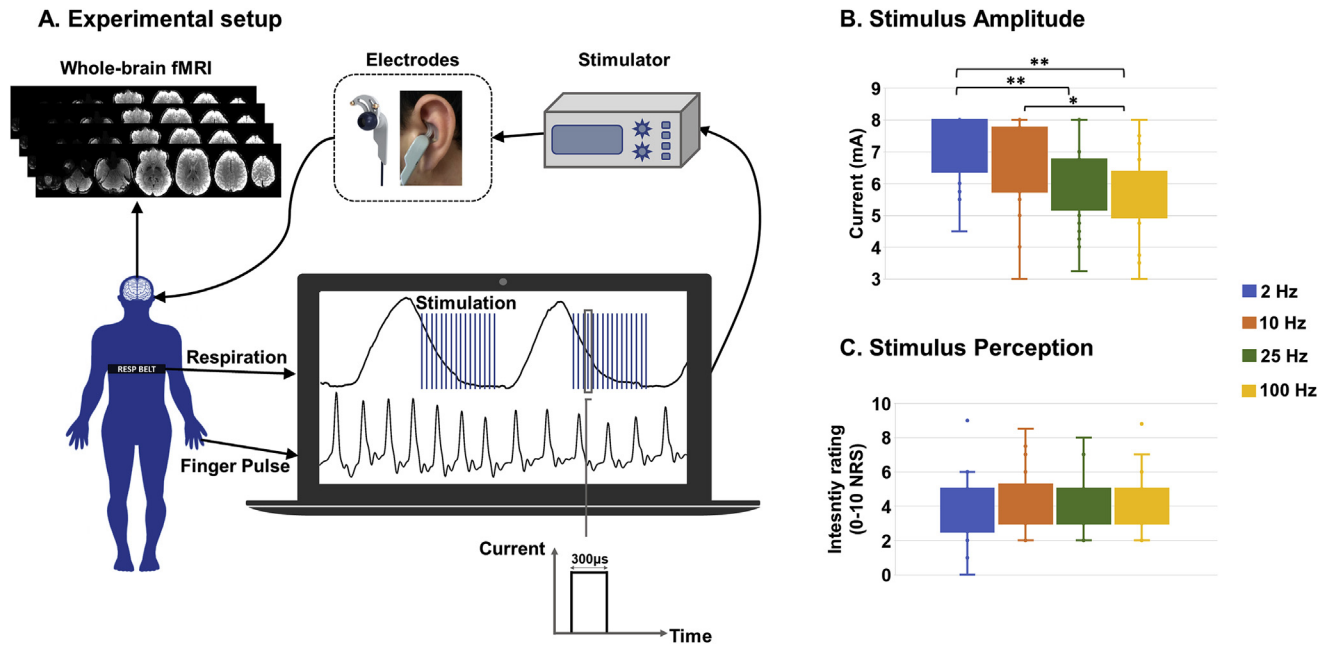
Fig. 1. (A) Experimental setup for data collection: fMRI data were collected with whole-brain coverage, concurrently with finger pulse and respiration signals; the latter was used to trigger in real-time the onset of respiration-gated left auricular vagal stimulation, delivered through custom electrodes placed over the cymba conchae of the ear. (B) Stimulation amplitude (current, mA) significantly decreased with increasing frequencies (** = p < 0.01, * = p < 0.05; Bonferroni-corrected for multiple comparisons), for targeted and (C) observed equivalent stimulus intensity ratings (no significant differences between frequencies were found, p = 0.676).

peak for improved annotation compared to the pulse oxygenation signal (i.e. SpO2), placed on the index finger of the right hand. Both finger pulse and respiration signals were collected at 400 Hz using a 16-channel Powerlab DAQ System (ADInstruments, Colorado Springs, CO, USA) and the LabChart Acquisition Software (ADInstruments) running on a conventional Windows OS laptop.

MRI data preprocessing

fMRI data preprocessing was performed using a combination of tools provided by the Oxford Center for Functional MRI of the Brain (FMRIB) Software Library (FSL; v. 5.0.7), the Analysis of Functional NeuroImages (AFNI), and in-house bash scripts. Preprocessing steps included correction for cardiorespiratory noise (RETROICOR), slice timing (using a custom script accounting for the Simultaneous Multi-Slice acquisition of the dataset), susceptibility-induced distortion (estimated using topup, FSL), and head motion (MCFLIRT, FSL). Framewise displacement (FD) was calculated for each scan run, and runs with maximum FD exceeding 2 mm were excluded from further analyses (Fig. 2). The T1-weighted anatomical dataset was then normalized to an MNI template (ICBM 2009a Nonlinear Asymmetric template [32]), using linear and nonlinear transformations (FSL FLIRT and FNIRT, respectively). A brainstem mask defined in the ICBM152 MNI space (and used in our own and others' prior studies [7,26,33–35]), was transformed into individual functional spaces by inverting the estimated transform matrices, and applying this inverted transform to the functional data. Spatial smoothing was carried out using a Gaussian kernel with FWHM = 3 mm.

Brainstem-focused fMRI data analyses

First-level General Linear Model (GLM) analyses were carried out for each subject and each scan run using an event-related design and the fMRI Expert Analysis Tool (FEAT v6.00, FSL). For each scan run, stimulation timings (recorded via Labview computer) were convolved with a set of three basis functions chosen by

the FMRIB's Linear Optimal Basis Set (FLOBS, FSL) algorithm to account for the potential deviation of the brainstem response from the canonical hemodynamic impulse response function as well as the systematic influence of hemodynamic response to the prior exhalation/stimulus event, as in our previous brainstem-focused analyses [26]. Additional regressors of no interest were used for censoring of motion outliers (as estimated through the fsl_motion_outliers tool) and for cardiogenic pulsatility reduction in fMRI signals by convolving heart rate with the previously-reported cardiac response function [36].

Single-subject parameter estimates (PEs) for each basis function were then combined into a signed root mean square (RMS) summary statistic [37], normalized to MNI space and concatenated for the subsequent group-level analyses. Given the high non-Gaussian distribution of the summary statistics, second-level analyses were carried out using nonparametric permutation analysis (5000 randomizations; randomise, FSL). Brainstem responses were evaluated by comparing each active stimulation condition with the sham stimulation run (which also controls for general respiratory modulation of the fMRI signal), using paired nonparametric randomization tests. Two sets of analyses were performed (Fig. 2). As in our previous work [26], a search volume defined in the ipsilateral (left) dorsal medulla was applied to evaluate responses at the site of primary synapse for vagal afference, e.g. NTS. Significance within this small-volume search space was set at uncorrected p < 0.05, due to the limited signal-to-noise ratio (SNR) typical for brainstem responses [30,33,38]. Two brainstem atlases — Duvernoy's Atlas of the Human Brain Stem and Cerebellum [39] and Olszewski and Baxter's Cytoarchitecture of Human Brainstem [40] — aided the localization of significant fMRI clusters. In the second analysis, a region of interest (ROI) approach was used to evaluate the same contrasts in specific neurotransmitter/neuromodulator source nuclei previously hypothesized to be modulated by taVNS. These included bilateral locus coeruleus (LC), dorsal and median raphe nuclei (DR, MR), and periaqueductal gray (PAG), defined in MNI space using the Harvard Ascending Arousal Network Atlas (AAN
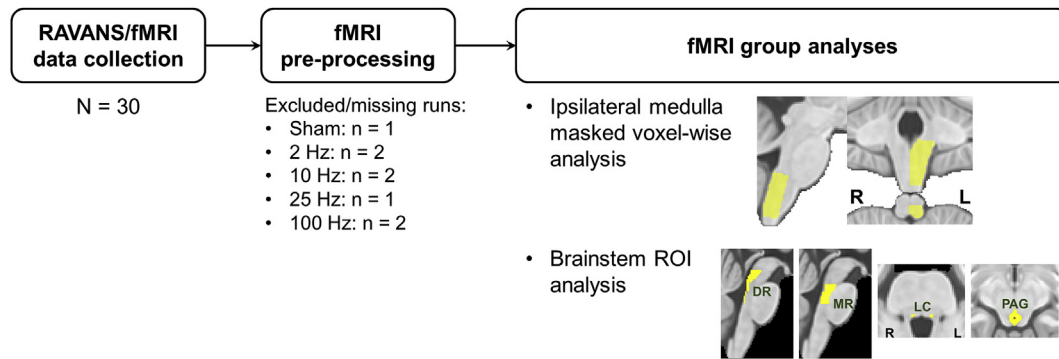
Fig. 2. Schematic of RAVANS/fMRI data analysis. From the initial N = 30 cohort, 5 runs per subject were collected and checked for sufficient quality in the pre-processing stage. Two main analyses were performed: 1) voxel-wise analysis restricted to the ipsilateral medulla (i.e. site of ipsilateral NTS); 2) ROI analysis investigating the involvement of important pontine and midbrain neurotransmitter/neuromodulator source nuclei.

(Edlow et al., 2012)). For each of these nuclei, an Extent/Activation Index (EAI) was defined as follows:

$$EAI_{ROI} = \overline{sumstat_{p\,<\,0.05}} \times \frac{\#\,voxels_{p\,<\,0.05}}{\#\,ROI\,voxels} \times 100$$

The EAI, introduced for brainstem ROI analyses in our previous paper [26], prevents very significant but spatially limited (i.e., a few voxels) activations from driving the outcome metric, using a multiplicative factor calculated at the group level for each contrast (RAVANS − Sham) to weigh the average value of the summary statistics extracted at the single subject level. The EAI indices for the different ROIs were then compared across different stimulus frequencies using linear mixed-effects models. Appropriate statistical contrasts were defined to test for significant effects of each frequency, as well as for pairwise comparisons. Significance was set at $p < 0.05$.

Cardiovagal response analysis using HF-HRV

For HF-HRV analysis, finger pulse time-series for each run were first annotated to identify peaks using an automated in-house algorithm followed by manual inspection for confirmation. Continuous (real-time) spectral measures of heart rate variability (HRV) were then estimated from this annotation time-series using a statistical, point-process method [41] described and used in several of our previous studies [26,35,42–44]. The power within the high-frequency band (HF-HRV, 0.15–0.40 Hz) was chosen as a metric for cardiovagal modulation. For analysis, the HF-HRV time-series amplitude was averaged over the entire scan run, and RAVANS-Sham differences were calculated for all stimulation frequencies and for each individual. We also used a linear regression analysis to assess correlation between HF-HRV response and EAI values for the ROIs defined above (i.e., DR, MR, LC, PAG) (significant at $p < 0.05$).

taVNS effect on respiratory parameters

In a separate analysis, the potential effect of taVNS delivered at different frequencies on respiratory parameters — namely, relative amplitude and frequency — was assessed. For each respiratory signal, inhalation peaks and exhalation troughs were automatically annotated in Matlab, and visually inspected to correct for mis-annotations. Mean amplitude, as measured by peak-to-trough voltage variations, was calculated for each taVNS stimulation frequency and sham stimulation condition. The belt was placed in identical position across taVNS stimulation runs for each subject, allowing for calculation of relative mV amplitude difference between stimulation and sham runs, reflecting potential differences in respiratory volume. Mean respiratory frequency was also estimated for each run and subject. Linear mixed-effects models were fitted to the data using taVNS (both active and sham) as a predictor, and significant effects were assessed using ANOVA testing followed by post-hoc pairwise comparisons when appropriate.

Results

The taVNS stimulation was well-tolerated by all subjects across frequencies, and experiments were completed without significant adverse events. Our choice of percept-matching stimulation intensity led to significantly different current intensity levels used across the different frequencies (F-score = 10.26, $p < 0.001$), with generally higher current intensities used for lower frequency values (Fig. 1, Table 1). Post-hoc t-tests (Bonferroni-corrected for multiple comparisons) revealed significantly higher current levels for 2 Hz RAVANS taVNS compared to 25 Hz RAVANS ($p < 0.001$) and 100 Hz RAVANS ($p < 0.001$), as well as for 10 Hz RAVANS compared to 100 Hz RAVANS ($p = 0.027$). As expected, due to our percept-matching procedure, no differences were found for stimulus intensity ratings, as subjects reported mean percept intensity values close to 4 (on a scale from 0 to 10) across the different frequencies (see Table 1 for mean ± SD values).

Despite the reduced current intensity levels evident for 100 Hz, brainstem medullary responses for each stimulation frequency compared to the Sham condition (Fig. 3) demonstrated robust response in ipsilateral medulla for 100 Hz RAVANS taVNS (the correspondent slice from the Duvernoy atlas is overlaid to the activation in order to aid localization). The ipsilateral activation cluster encompassed purported NTS, as well as DMNX, spinal trigeminal nucleus (SpV), nucleus gracilis (NGr), nucleus cuneatus (NCun), and a portion of the reticular formation including NAmb and pre-Bötzinger complex (pBötzi). A smaller activation cluster, in a similar location, was found in response to 2 Hz RAVANS stimulation. In order to compare the medullary responses in an unbiased fashion, a group analysis contrasting all stimulation frequencies to

Table 1
Stimulation currents and subjects' perceptual intensity ratings for the different frequencies of RAVANS taVNS stimulation (mean ± SD).

Frequency (Hz)	Current (mA)	Intensity (0–10 NRS)
2	7.18 ± 0.95	3.93 ± 1.66
10	6.46 ± 1.30	4.38 ± 1.60
25	5.93 ± 1.21	4.35 ± 1.47
100	5.57 ± 1.18	4.30 ± 1.49

Sham was performed, and the resulting ipsilateral medulla cluster was transformed into a binary ROI mask. The EAI within this ROI was then computed for each stimulation frequency and subject. A direct comparison then found significantly higher EAI values for 100 Hz stimulation compared to all other stimulation frequencies (F-score = 15.3, p≪0.001 followed by Bonferroni-corrected post-hoc t-tests).

In pontine and midbrain ROI analyses, RAVANS (compared to Sham) delivered at 100 Hz was consistently found to evoke a robust fMRI response (quantified by EAI) for all nuclei of interest (Fig. 4A). Significantly higher EAI values were found for 100 Hz RAVANS compared to Sham for all considered ROIs (DR: 547.24 ± 227.35 a.u., p = 0.003; MR: 137.81 ± 86.91 a.u., p = 0.004; left LC: 29.77 ± 20.22 a.u., p = 0.007; right LC: 518.01 ± 210.24 a.u., p = 0.001; PAG: 110.83 ± 38.13 a.u., p < 0.001), and for 2 Hz RAVANS compared to Sham for DR (371.21 ± 127.87 a.u., p = 0.035) and right LC (339.18 ± 106.73 a.u., p = 0.021). Furthermore, 100 Hz RAVANS evoked significantly higher responses compared to 10 Hz and 25 Hz in DR (100 Hz vs 10 Hz: p = 0.001; 100 Hz vs 25 Hz: p < 0.001) and right LC (100 Hz vs 10 Hz: p < 0.001; 100 Hz vs 25 Hz: p < 0.001), and compared to all other frequencies in PAG (100 Hz vs 2 Hz: p = 0.016; 100 Hz vs 10 Hz: 0.004; 100 Hz vs 25 Hz: p < 0.001). Finally, EAI values for RAVANS delivered at 2 Hz were significantly higher than 10 Hz stimulation in right LC (p = 0.022), and than 25 Hz stimulation in DR (p = 0.027) and right LC (p = 0.022). Exploratory intersubject heterogeneity analyses were also carried out to investigate whether EAI values for a given brainstem ROI were correlated across different stimulation frequencies. Results showed significant correlations between 2 Hz and 100 Hz EAI values in DR (Pearson's r = 0.40, p-value = 0.039; Fig. 4B) and in right LC (r = 0.51, p-value = 0.006; Fig. 4C). Thus, subjects demonstrating higher responses in these nuclei for 2 Hz RAVANS, also showed higher responses for 100 Hz RAVANS.

We also completed a HF-HRV analysis to explore cardiovagal response to RAVANS taVNS at different frequencies. We found that compared to Sham, the HF-HRV power was increased for 2 and 100 Hz RAVANS (2 Hz - Sham: 119.45 ± 1280.37 ms^2; 100 Hz - Sham: 123.95 ± 751.81 ms^2), and decreased for 10 and 25 Hz stimulation (10 Hz - Sham: 103.03 ± 1032.06 ms^2; 25 Hz - Sham: 179.22 ± 922.98 ms^2). However, these responses were not significantly different, using a mixed-effects model, likely due to the high inter-subject variability of the HF-HRV index. Finally, an exploratory correlation analysis revealed a significant correlation (Pearson's r = 0.55, p-value = 0.006) between individuals' HF-HRV change scores from Sham and EAI values in right LC for RAVANS delivered at 100 Hz. Thus, subjects with greater fMRI response in this noradrenergic source nucleus also demonstrated greater cardiovagal modulation at this stimulation frequency. We also looked at average heart rate (HR) values over active versus Sham conditions, and found minimal, non-significant average increases for all conditions (2 Hz - Sham: 0.56 ± 2.91 beats/minute (bpm); 10 Hz - Sham: 1.41 ± 4.31 bpm; 25 Hz - Sham: 1.19 ± 3.65 bpm; 100 Hz - Sham: 0.79 ± 3.45 bpm).

Finally, no significant effect of RAVANS stimulus frequency on respiratory amplitude (F-score = 0.725, p = 0.539) or respiratory frequency (F-score = 2.058, p = 0.110) was found. Mean respiratory amplitudes and frequencies changes from Sham are reported in Table 2 for each condition.

Discussion

The therapeutic potential of taVNS is currently being explored for numerous clinical applications. However, optimized response for different clinical indications may depend on specific neuromodulation parameters, and systematic assessments of their influence are still needed to optimize the effects of this promising approach. Our study followed up on our previous work demonstrating enhanced brainstem response to taVNS delivered in the cymba conchae of the left ear during the exhalation phase of respiration (RAVANS [4,7,26]), and characterized the brainstem
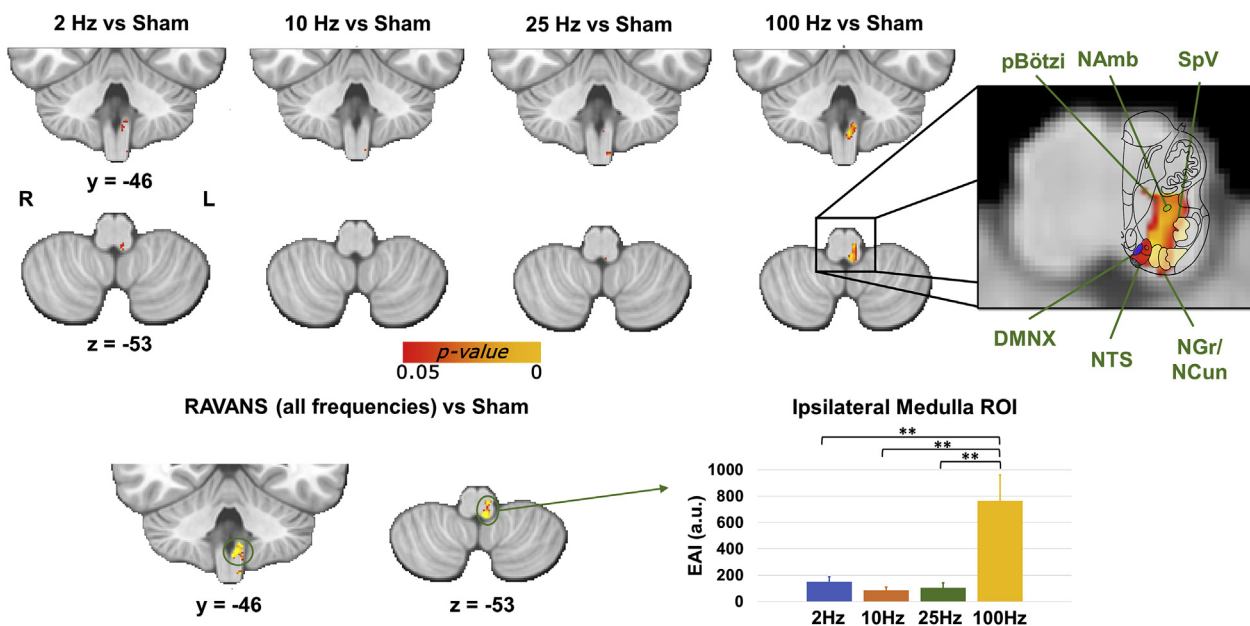

Fig. 3. Top: group maps showing ipsilateral medullary responses to RAVANS taVNS delivered at different stimulation frequencies (note: fMRI response for respiration-gated Sham was subtracted from each active stimulation condition in order to control for respiratory modulation of the fMRI signal). Inset: enlarged medullary response to 100 Hz eRAVANS is compared to the corresponding brainstem slice from the Duvernoy's atlas to aid the localization of functional responses. The activation cluster was consistent with purported NTS, but also encompassed DMNX, NAmb, pBötzi, SpV, and NGr/NCun nuclei. Bottom: A similar ipsilateral medulla ROI resulting from contrasting all RAVANS frequencies (to avoid bias) versus Sham was used to directly compare EAI values for the different stimulation frequencies. Significantly greater fMRI response was found for 100 Hz stimulation compared to all other frequencies. ** = p < 0.001; error bars show SEM.

A. Brainstem ROI analysis – EAI index
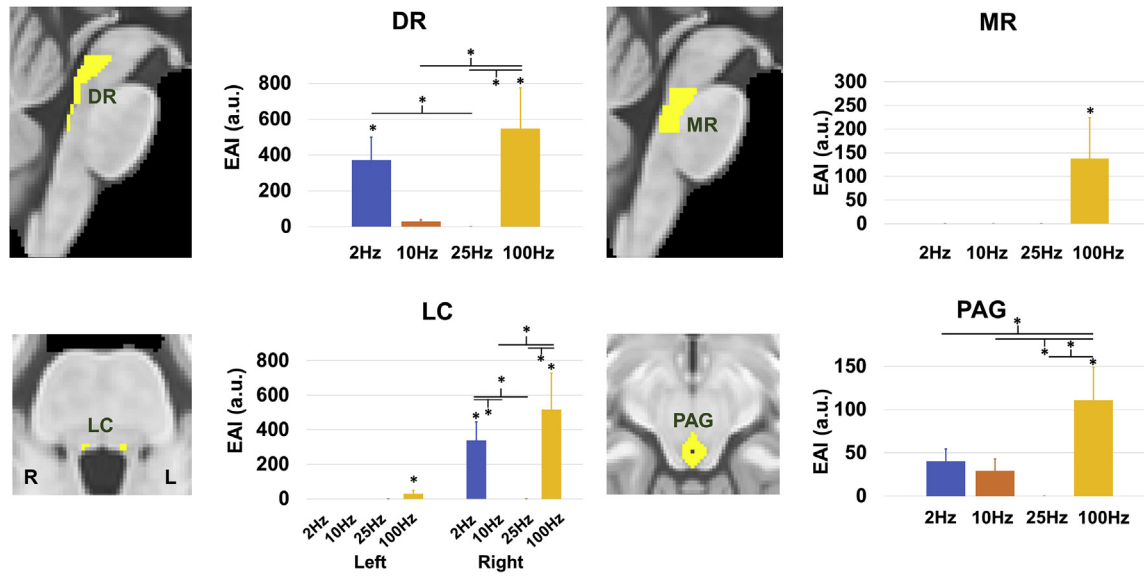
B. DR EAIs (2Hz vs 100Hz)
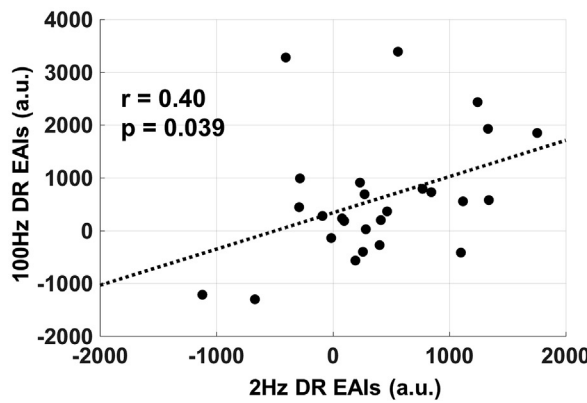
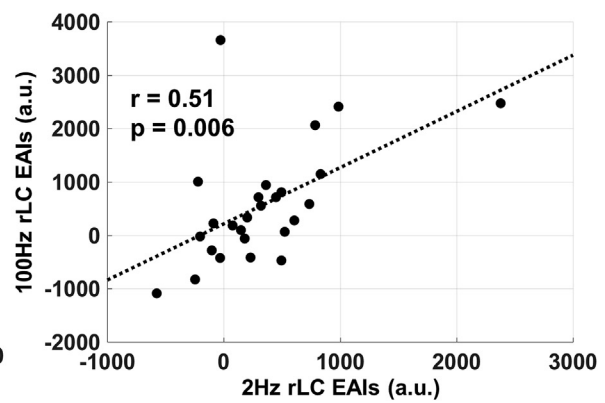## C. Right LC EAIs (2Hz vs 100Hz)

Fig. 4. (A) Brainstem ROI analysis found that RAVANS delivered at 100 Hz produced the highest fMRI responses in serotonergic (DR, MR) and noradrenergic (LC) source nuclei, as well as in the PAG, and important region for pain and autonomic modulation. Analyses used an Extent/Activation Index (EAI), which weighted the activation strength by its extent within the total ROI volume (error bars show SEM). DR and LC also showed fMRI response to 2 Hz RAVANS, and significant positive correlations were found between individuals' EAI values at 2 Hz and 100 Hz for both DR (B) and right LC (C). Thus, subjects with higher responses to 2 Hz RAVANS also showed higher responses to 100 Hz RAVANS in these nuclei.

response to RAVANS taVNS delivered at four different stimulation frequencies (2 Hz, 10 Hz, 25 Hz, 100 Hz). Using fMRI, we evaluated event-related response in the NTS, which is the site of the primary synapse for afferent vagal fibers, as well as in other brainstem nuclei involved in autonomic, pain, and monoaminergic regulation. Compared to Sham stimulation, we found that RAVANS delivered at 100 Hz evoked the strongest response in a cluster located in the left (ipsilateral) medulla and consistent with purported NTS. A co-localized although weaker response was found for 2 Hz RAVANS. When directly compared using the EAI index, fMRI activation in the ipsilateral medulla in response to 100 Hz RAVANS demonstrated significantly greater activation compared to lower frequencies of stimulation.

Our ROI analysis used previously published standard space atlas definitions for important monoamine neurotransmitter source nuclei (LC, noradrenergic; MR, DR, serotonergic) and pain/homeostatic regulation nuclei such as the PAG. The results showed that RAVANS delivered at 100 Hz consistently evoked higher responses (as measured by the EAI index) in these ROIs. Mirroring the medullary

results, significant, however lower in magnitude, fMRI responses were also found for 2 Hz RAVANS in DR and right LC. Taken together, our voxelwise and ROI fMRI results support previous localization of taVNS targeting in the human brainstem, and demonstrate the significant influence of the stimulation frequency on the circuitry involved. Moreover, these results suggest a nonlinear relationship between stimulation frequency and brainstem response, where the total energy for delivered current is not the main factor driving the effects of RAVANS. Thus, brainstem responses do not monotonically decrease with decreasing stimulation frequency, and may instead follow a U-shaped response pattern across the commonly applied stimulation frequency range for many brainstem nuclei.

In addition to purported ipsilateral NTS, stimulus-evoked response to RAVANS delivered at 100 Hz encompassed a wider cluster in the dorsomedial and medial medulla, which included purported DMNX, NAmb, pBötzi, SpV, and NGr/NCun. NAmb and DMNX are the main premotor nuclei for vagal outflow to the heart and the gastrointestinal tract, respectively. However, both nuclei are known to receive afferent projections from NTS [45−47], and

Table 2
Effect of RAVANS stimulation frequency on respiratory amplitude (as calculated from peak-to-trough voltage differences) and respiratory frequency (breaths per minute) changes versus Sham.

RAVANS Frequency	Respiratory Amplitude Change (mV)	Respiratory Frequency Change (Breaths/Minute)
2 Hz	0.013 ± 0.054	-0.655 ± 1.188
10 Hz	0.018 ± 0.083	-0.821 ± 1.836
25 Hz	0.004 ± 0.058	-0.249 ± 1.165
100 Hz	0.001 ± 0.041	-0.327 ± 1.253

their modulation in response to RAVANS might be due to vago-vagal feedback and serve as the basis of therapeutic effects observed for cardiovascular [14,16,48] and gastrointestinal [11,12] taVNS applications. The pre-Bötzinger complex, a functionally-defined region located ventrally to the NAmb, is known to be a generator for respiratory rhythms in mammals [49], and evoked fMRI response in this nuclei may result from the respiratory-gated nature of RAVANS taVNS, which future studies should explore more explicitly. Finally, RAVANS delivered at 100 Hz also evoked fMRI response in nuclei involved in relaying sensory afference, namely SpV and dorsal column nuclei (NGr/NCun). SpV activation in response to RAVANS is consistent with previous findings from our group [26]. SpV is the main nucleus for trigeminal sensory afference from the head, and a recent study suggested the existence of a "trigeminovagal complex" in the human medulla, where afferent vagus and trigeminal systems connect anatomically [50]. More surprisingly, our response cluster possibly extends to the dorsal column nuclei, namely gracilis and cuneatus, known to relay touch and proprioceptive afference from the lower and upper body, respectively [46]. A possible explanation for their involvement can be found in a recent study by Mahadi and coauthors [51], who investigated the central projections from nerves innervating the tragus in rats. Their findings showed dense labeling in the cervical spinal cord, as well as sensory nuclei in the medulla, thus suggesting the existence of a spinal cervical sensory pathway for tragus electrical stimulation effects. In humans, the tragus has been shown to be innervated by both the ABVN and the greater auricular nerve (GAN), while the cymba conchae, the stimulation site of the present study, is more consistently and uniquely innervated by the ABVN [52]. However, anatomical variability in innervation patterns, or sensory perception quality of different stimulation frequencies — anecdotally, 100 Hz RAVANS was commonly described as "vibrational", as opposed to 2 Hz RAVANS, which was more commonly described with terms such as "needling" — might contribute to the involvement of both sensory pathways.

A similar response pattern to different RAVANS frequencies was found in the brainstem ROI analysis, where 100 Hz RAVANS evoked the highest responses in all considered nuclei, and significant, although lower, responses to 2 Hz RAVANS in DR and right LC. In these nuclei, interestingly, significant correlations were found between individual EAI values for 100 Hz and 2 Hz, supporting the connection hypothesized in our previous study between a more robust NTS targeting and a greater activation of these higher pontine/midbrain nuclei [26]. In addition to confirming the engagement of serotonergic and noradrenergic source nuclei in response to RAVANS, the present study also found a significant response of the PAG to 100 Hz stimulation. This columnar region contains neurons associated with multiple neurotransmitter systems, and involved in survival-related responses and homeostatic regulation important for affective responses, nociception, and stress [53]. Afferents to the PAG arise from the hypothalamus, the brainstem reticular formation, NTS, raphe nuclei, LC, and the spinal cord [46,54]. Its successful targeting by taVNS might suggest a possible mechanism underlying analgesic effects of RAVANS therapy, as has been previously shown by our group [4].

Several groups have suggested HRV response to stimulation as a potential biomarker for taVNS stimulation [13,55]. While our prior 7T fMRI/HF-HRV study reported an interesting evoked response to stimulation for HF-HRV [26], our current study, with a larger sample size, did not find a similar evoked response. Moreover, changes in HF-HRV over the entire stimulus run, compared to Sham, demonstrated increased cardiovagal modulation for 100 Hz, but with such high inter-subject variability that a statistically significant effect was not found. However, we should note that our study was performed in healthy adults and more robust effects may be found for clinical populations with noted dysfunction in HRV parameters. Similar to brainstem fMRI results, relative to no-stimulation control, HF-HRV power was increased on average for 2 Hz and 100 Hz stimulation, while average HF-HRV power was decreased for the other frequencies (10 Hz and 25 Hz). Previous papers have also explored the influence of stimulation parameters on various cardiac outcomes. For example, Badran and co-authors delivered continuous taVNS combining 3 different pulse widths and 3 different frequencies, and found that the greatest effect on heart rate was provided by taVNS delivered at 10 Hz with a 500 μs pulse width [16]. With our fMRI design, we only explored one parameter, stimulus frequency, and were only able to sample the parameter space at 4 different frequencies. Future studies devoted to expanding the exploration of taVNS stimulus-response space should be welcomed, including modeling efforts allowing for finer sampling of such space.

Finally, stimulation frequency was found to have no effect on respiration depth or rhythm, for all frequencies examined in the present study. Subjects were not informed of the respiratory-gated nature of RAVANS taVNS, and post-scan qualitative assessments revealed that subjects remained blinded to the respiratory gating even after having experienced it. This suggests that respiration was not modulated due to both direct physiological influences nor volitional respiratory modulation due to stimulus anticipation.

Although we controlled for multiple factors known to reduce signal in brainstem fMRI data — e.g., correcting for physiological noise, masking the brainstem prior to smoothing to reduce the impact of cardiac pulsation noise, controlling for respiratory-related fluctuations by subtracting fMRI response for the Sham condition — our current study was performed at 3T and not with ultrahigh-field MRI (7T) as in our previous study. This certainly played a role in limiting our spatiotemporal resolution and signal-to-noise ratio, however, our current study was performed with greater sample size (N = 30 vs N = 16 in Ref. [26]) in an attempt to maintain comparable power with our previous study.

In conclusion, our RAVANS fMRI study demonstrated that stimulation frequency has a considerable effect on brainstem responses, with 100 Hz stimulation evoking the most robust activation in ipsilateral NTS and up-stream pain/autonomic modulatory and monoaminergic source nuclei. These results suggest that stimulation frequency should be taken into account when devising clinical applications for taVNS, and fMRI could be used to evaluate specific circuitry response to taVNS applied with variable stimulation parameters.

Declaration of competing interest

CRediT authorship contribution statement

Roberta Sclocco: Conceptualization, Methodology, Investigation, Formal analysis, Writing - original draft, Visualization. **Ronald G. Garcia:** Conceptualization, Investigation, Writing - review & editing. **Norman W. Kettner:** Conceptualization, Writing - review & editing. **Harrison P. Fisher:** Investigation, Project administration, Formal analysis, Writing - review & editing. **Kylie Isenburg:** Investigation, Project administration, Writing - review & editing. **Maya Makarovsky:** Formal analysis. **Jessica A. Stowell:** Investigation, Project administration. **Jill Goldstein:** Conceptualization, Writing - review & editing. **Riccardo Barbieri:** Methodology, Writing - review & editing. **Vitaly Napadow:** Conceptualization, Writing - review & editing, Supervision, Funding acquisition.

Acknowledgements

References

[1] Ventureyra EC. Transcutaneous vagus nerve stimulation for partial onset seizure therapy. A new concept. Child's Nerv Syst ChNS Off J Int Soc Pediatr Neurosurg 2000;16(2):101–2.

[2] Rong P-J, et al. Transcutaneous vagus nerve stimulation for the treatment of depression: a study protocol for a double blinded randomized clinical trial. BMC Compl Alternative Med 2012;12(1):255.

[3] Hein E, et al. Auricular transcutaneous electrical nerve stimulation in depressed patients: a randomized controlled pilot study. Vienna, Austria J Neural Transm 1996;120(5):821–7. 2013.

[4] Napadow V, et al. Evoked pain analgesia in chronic pelvic pain patients using respiratory-gated auricular vagal afferent nerve stimulation. Pain Med 2012;13(6):777–89.

[5] Laqua R, et al. Transcutaneous vagal nerve stimulation may elicit anti-and pronociceptive effects under experimentally-induced pain—a crossover placebo-controlled investigation. Auton Neurosci 2014;185:120–2.

[6] Straube A, et al. Treatment of chronic migraine with transcutaneous stimulation of the auricular branch of the vagal nerve (auricular t-VNS): a randomized, monocentric clinical trial. J Headache Pain 2015;16:543.

[7] Garcia RG, et al. Modulation of brainstem activity and connectivity by respiratory-gated auricular vagal afferent nerve stimulation in migraine patients. Pain 2017;158(8):1461–72.

[8] Janner H, et al. Effects of electrical transcutaneous vagus nerve stimulation on the perceived intensity of repetitive painful heat stimuli: a blinded placebo- and sham-controlled randomized crossover investigation. Anesth Analg 2018;126(6):2085–92.

[9] Redgrave JN, et al. Transcutaneous auricular vagus nerve stimulation with concurrent upper limb repetitive task practice for poststroke motor recovery: a pilot study. J Stroke Cerebrovasc Dis 2018;27(7):1998–2005.

[10] Zhao B, et al. Transcutaneous auricular vagus nerve stimulation in treating post-stroke insomnia monitored by resting-state fMRI: the first case report. Brain Stimul 2019;12(3):824–6.

[11] Gao XY, et al. Investigation of specificity of auricular acupuncture points in regulation of autonomic function in anesthetized rats. Auton Neurosci 2008;138(1–2):50–6.

[12] Hong GS, et al. Effect of transcutaneous vagus nerve stimulation on muscle activity in the gastrointestinal tract (transVaGa): a prospective clinical trial. Int J Colorectal Dis 2019;34(3):417–22.

[13] Clancy JA, et al. Non-invasive vagus nerve stimulation in healthy humans reduces sympathetic nerve activity. Brain Stimul 2014;7(6):871–7.

[14] Antonino D, et al. Non-invasive vagus nerve stimulation acutely improves spontaneous cardiac baroreflex sensitivity in healthy young men: a randomized placebo-controlled trial. Brain Stimul 2017;10(5):875–81.

[15] Sclocco R, et al. Respiratory-gated auricular vagal afferent nerve stimulation (RAVANS) effects on autonomic outflow in hypertension. Conf Proc IEEE Eng Med Biol Soc 2017;2017:3130–3.

[16] Badran BW, et al. Short trains of transcutaneous auricular vagus nerve stimulation (taVNS) have parameter-specific effects on heart rate. Brain Stimul 2018;11(4):699–708.

[17] Fisher, H., et al. Acute effects of respiratory-gated auricular vagal afferent nerve stimulation (RAVANS) in the modulation of blood pressure in hypertensive patients in 2018 computing in cardiology conference (CinC). 2018. IEEE.

[18] Tobaldini E, et al. Cardiac and peripheral autonomic responses to orthostatic stress during transcutaneous vagus nerve stimulation in healthy subjects. J Clin Med 2019;8(4).

[19] Kaniusas E, et al. Current directions in the auricular vagus nerve stimulation I - a physiological perspective. Front Neurosci 2019;13:854.

[20] Kaniusas E, et al. Current directions in the auricular vagus nerve stimulation II - an engineering perspective. Front Neurosci 2019;13:772.

[21] Kraus T, et al. CNS BOLD fMRI effects of sham-controlled transcutaneous electrical nerve stimulation in the left outer auditory canal - a pilot study. Brain Stimul 2013;6(5):798–804.

[22] Frangos E, Ellrich J, Komisaruk BR. Non-invasive access to the vagus nerve central projections via electrical stimulation of the external ear: fMRI evidence in humans. Brain Stimul 2015;8(3):624–36.

[23] Yakunina N, Kim SS, Nam EC. Optimization of transcutaneous vagus nerve stimulation using functional MRI. Neuromodulation 2017;20(3):290–300.

[24] Badran BW, et al. Neurophysiologic effects of transcutaneous auricular vagus nerve stimulation (taVNS) via electrical stimulation of the tragus: a concurrent taVNS/fMRI study and review. Brain Stimul 2018;11(3):492–500.

[25] Wang Z, et al. Frequency-dependent functional connectivity of the nucleus accumbens during continuous transcutaneous vagus nerve stimulation in major depressive disorder. J Psychiatr Res 2018;102:123–31.

[26] Sclocco R, et al. The influence of respiration on brainstem and cardiovagal response to auricular vagus nerve stimulation: a multimodal ultrahigh-field (7T) fMRI study. Brain Stimul 2;12(4):911–21.

[27] Sun J, et al. Transcutaneous auricular vagus nerve stimulation (taVNS) have stimulus waveform specific effects on brain responses: fMRI evidence in humans. Brain Stimul Basic Trans Clin Res Neuromodulation 2019;12(2):575.

[28] Rangon CM. Reconsidering sham in transcutaneous vagus nerve stimulation studies. Clin Neurophysiol 2018;129(11):2501–2.

[29] Keute M, Ruhnau P, Zaehle T. Reply to "reconsidering sham in transcutaneous vagus nerve stimulation studies. Clin Neurophysiol 2018;129(11):2503–4.

[30] Sclocco R, et al. Challenges and opportunities for brainstem neuroimaging with ultrahigh field MRI. Neuroimage 2018;168:412–26.

[31] Napadow V, Sclocco R, Henderson LA. Brainstem neuroimaging of nociception and pain circuitries. Pain Rep 2019;4(4):e745.

[32] Fonov V, et al. Unbiased average age-appropriate atlases for pediatric studies. Neuroimage 2011;54(1):313–27.

[33] Beissner F, Baudrexel S. Investigating the human brainstem with structural and functional MRI. Front Hum Neurosci 2014;8:116.

[34] Moher Alsady T, Blessing EM, Beissner F. MICA—a toolbox for masked independent component analysis of fMRI data. Hum Brain Mapp 2016;37(10):3544–56.

[35] Sclocco R, et al. Neuroimaging brainstem circuitry supporting cardiovagal response to pain: a combined heart rate variability/ultrahigh-field (7 T) functional magnetic resonance imaging study. Philos Trans A Math Phys Eng Sci 2016;374. 2067.

[36] Chang C, Cunningham JP, Glover GH. Influence of heart rate on the BOLD signal: the cardiac response function. Neuroimage 2009;44(3):857–69.

[37] Calhoun VD, et al. fMRI analysis with the general linear model: removal of latency-induced amplitude bias by incorporation of hemodynamic derivative terms. Neuroimage 2004;22(1):252–7.

[38] Brooks JC, et al. Physiological noise in brainstem FMRI. Front Hum Neurosci 2013;7:623.

[39] Naidich TP, et al. Duvernoy's atlas of the human brain stem and Cerebellum. Vienna: Springer Vienna; 2009.

[40] Olszewski J, Baxter D. Cytoarchitecture of the human brain stem. Cytoarchitecture of the human brain stem.; 1954.

[41] Barbieri R, et al. A point-process model of human heartbeat intervals: new definitions of heart rate and heart rate variability. Am J Physiol Heart Circ Physiol 2005;288(1):H424–35.

[42] Napadow V, et al. Brain correlates of autonomic modulation: combining heart rate variability with fMRI. Neuroimage 2008;42(1):169–77.

[43] Sclocco R, et al. Brain circuitry supporting multi-organ autonomic outflow in response to nausea. 2014. Cerebral Cortex (New York, N.Y.: 1991).

[44] Valenza G, et al. The central autonomic network at rest: uncovering functional MRI correlates of time-varying autonomic outflow. Neuroimage 2019;197: 383—90.

[45] Nomura S, Mizuno N. Central distribution of primary afferent fibers in the Arnold's nerve (the auricular branch of the vagus nerve): a transganglionic HRP study in the cat. Brain Res 1984;292(2):199—205.

[46] Parent A. Carpenter's human neuroanatomy. Williams & Wilkins; 1996.

[47] Kiyokawa J, et al. Origin, course and distribution of the nerves to the posterosuperior wall of the external acoustic meatus. Anat Sci Int 2014;89(4): 238—45.

[48] Stowell J, et al. Dose-optimization of respiratory-gated auricular vagal afferent nerve stimulation (RAVANS) for blood pressure modulation in hypertensive patients. Comput Cardiol 2019:1—4.

[49] Smith JC, et al. Pre-Botzinger complex: a brainstem region that may generate respiratory rhythm in mammals. Science 1991;254(5032):726—9.

[50] Henssen D, et al. Visualizing the trigeminovagal complex in the human medulla by combining ex-vivo ultra-high resolution structural MRI and polarized light imaging microscopy. Sci Rep 2019;9(1):11305.

[51] Mahadi K, et al. Cardiovascular autonomic effects of transcutaneous auricular nerve stimulation via the tragus in the rat involve spinal cervical sensory afferent pathways. Brain Stimul 2019;12(5):1151—8.

[52] Peuker ET, Filler TJ. The nerve supply of the human auricle. Clin Anat 2002;15(1):35—7.

[53] Bandler R, et al. Central circuits mediating patterned autonomic activity during active vs. passive emotional coping. Brain Res Bull 2000;53(1):95—104.

[54] Herbert H, Saper CB. Organization of medullary adrenergic and noradrenergic projections to the periaqueductal gray matter in the rat. J Comp Neurol 1992;315(1):34—52.

[55] Colzato LS, et al. Variable heart rate and a flexible mind: higher resting-state heart rate variability predicts better task-switching. Cognit Affect Behav Neurosci 2018;18(4):730—8.